Advanced Steel Construction – Vol. 19 No. 3 (2023) 262–272
DOI:10.18057/IJASC.2023.19.3.7

DISTRIBUTION OF RESIDUAL STRESS IN THE SPHERE-PIPE CONNECTION WELDS OF WELDED HOLLOW SPHERICAL JOINTS

Ren-Zhang Yan [1, 2], Chang-Long Zhang [1, 2], Shuai Wang [3], Jia-Qi Liu [2] and Tao Sun [4, *]

[1] *State Key Laboratory of Mountain Bridge and Tunnel Engineering, Chongqing Jiaotong University, Chongqing 400074, China*
[2] *School of Civil Engineering, Chongqing Jiaotong University, Chongqing 400074, China*
[3] *Chongqing Aerospace Polytechnic College, Chongqing 400021, China*
[4] *Department of Military Facility, Army Logistics Acadmy of PLA, Chongqing 401331, China*
[*] *(Corresponding author: Email: 372322119@qq.com)*

ABSTRACT

Welded hollow spherical joint is widely used in large-span spatial structures due to its simple structure, clear mechanical behavior and convenient connection. However, a large number of sphere-pipe connection welds at the joints will inevitably produce complex welding residual stress, which will have adverse effects on the stiffness of the joints and the overall safety of the structure. Focusing on the sphere-pipe connection welds on the hollow spherical joints, this paper keeps track of the whole process of sphere-pipe welding, analyzes and summarizes the distribution law and specific distribution mode of welding residual stress on the joints and parametrically analyzes the influence trend of the configuration dimension of joints on the distribution of welding residual stress. Studies have found that the circumferential welding residual tensile stress is mainly concentrated in and near the weld, while the compressive stress is concentrated in the outer area of the weld. The longitudinal residual stress shows the obvious bending features of external compression and internal tension along the wall thickness direction near the weld; The configuration dimension of the hollow spherical joint mainly affects the influence range of welding residual stress, that is, with the change of dimension, the welding heat-affected zone on steel pipes will vary within the area with a distance to the weld 0.6~1.35 times the diameter, and the heat-affected zone on spherical joints will vary within the area with a distance to the weld no more than 0.5 times the diameter. The above-mentioned refined research on the residual stress of the hollow spherical joint can lay a foundation for the accurate evaluation of the stiffness and overall safety of the welded hollow spherical joints.

ARTICLE HISTORY

Received: 12 October 2022
Revised: 27 April 2023
Accepted: 10 May 2023

KEYWORDS

Welded hollow spherical joint;
Welding residual stress;
Experiment;
Refined numerical simulation

1. Introduction

The welded hollow spherical joint is composed of a core hollow sphere welded with multiple steel pipes. Due to its simple structure, reliable force transmission, and convenient construction, it is widely used in large-span spatial grid structures. As we all know, since the welded hollow spherical joints are mainly made of steel [1], when the steel is welded, the welding area is under the action of highly concentrated heat, and the local steel will successively produce plastic expansion due to thermal compression and lead to uneven shrinkage deformation. At the same time, the microstructure and properties of the material have also changed greatly, and welding defects such as welding residual stress and residual deformation will inevitably occur in the welds and heat-affected zone [2]. These defects adversely affect on the stiffness, stability, brittleness and corrosion resistance of steel structure connections and joints [3], and even become the key factors restricting the selection of weld connection methods. The influence of welding residual stress on the connection of steel structures has been a hot topic of scholars. Osgood [4] first started to study welding residual stress and deformation in the 1920s and 1930s. Subsequently, scholars at home and abroad studied the distribution law of welding residual stress of welded joints and its influence on joint performance by combining experimental research and numerical simulation. Brar [5] precisely captured the residual stresses in heat affected zone of cruciform welded joint of hollow sectional pipes through finite element simulation. Wang [6] analyzed and clarified the high-temperature residual stress of the welded section of high-strength steel. Yang [7] studied the residual stress of high-performance steel after welding through experiments, and proposed a simple yet accurate method for determining the residual stress. Xu [8] compared and analyzed the residual stress of high-performance steel and high strength steel after welding. Mirzaee-Sisan [9] measured the circumferential and axial residual stresses of steel pipe butt welding. It can be seen from the above research results that, when the steel structure is welded, the distribution law of welding residual stress at the welded joint is relatively complex, and the influence on the connection performance of the steel structure cannot be ignored. Moreover, as the weld hollow spherical joint is a collection of multiple steel pipes, a large number of sphere-pipe welds are gathered. The influence of welding residual stress on the mechanical properties of hollow spherical joints is far worse than that of common welded joints. Sometimes the sphere-pipe joint weld becomes the cause of the overall collapse of the structure. For example, statistics of steel structure collapse accidents at home and abroad show that 19%~27% of the accidents are caused by joint failure [10]. The failure of the weld connection between the member pipe and the welded hollow sphere is one of the main reasons for the failure of the joint [11]. Therefore, in recent years, scholars at home and abroad have carried out a large number of studies on the mechanical properties of welded hollow spherical joints, such as stiffness, bearing capacity and influencing factors. Zang [12] analyzed the influence of the external ribs on the bearing capacity of welded hollow spherical joints. YU [13] studied the ultimate bearing capacity of ribbed hollow spherical joints and relationship with various influencing factors. CHEN [14] studied the ultimate bearing capacity and failure mechanism of welded hollow spherical joints through experiments. Some scholars studied the structural performance and ultimate bearing capacity of hollow spherical joints connected by rectangular steel pipes [15]. In terms of the stiffness research of welded hollow spherical joints, Liao [16], Liu [17], Lopez [18], Wang [19], Yan [20,21] have studied the stiffness calculation and analysis methods of welded hollow spherical joints. In addition, Liu [22,23] and Lu [24] studied the bearing capacity of welded hollow spherical joints after fire and high temperature action. Zhao [25~27] studied the influence of corrosion on the bearing capacity of welded hollow spherical joints. The above studies on the performance of welded hollow spherical joints do not consider the influence of welding residual stress. Only Zhao [28] analyzed the influence of welding residual stress on the mechanical behavior of hollow spherical joints through numerical simulation, but the material properties and welding process are simplified. The compression failure of welded hollow spherical joints is the stability failure of thin shells, and the welding residual stress will reduce the stiffness and stability of weldments. Therefore, the residual stress produced by the sphere-pipe weld has a significant influence on the stiffness and bearing capacity of the joints and furthermore, the overall safety of the spatial structure. In this paper, the commonly used welded hollow spherical joints in engineering are selected to study their variation laws of temperature field in the dynamic process of welding and determine the final distribution pattern of welding residual stress by combining experiment and numerical simulation, laying foundation for the fine analysis of mechanical properties of welded hollow spherical joints.

2. Design of welded hollow spherical joint sample

Hybrid structure of suspendome with stacked arch has been adopted in Chiping Gymnasium, Shandong, and the upper reticulated shell is in the form of welded hollow spherical joints. Complex residual stress tends to be generated in the hollow spherical joints due to lots of sphere-pipe welds, which greatly influences the stiffness and ultimate bearing capacity of the joints. In this paper, based on the project of suspendome in Chiping Gymnasium, Shandong, the

frequently used welded hollow spherical joints and circular steel pipes in the upper reticulated shell are selected as the research objects. Besides, in order to investigate the influence laws of the hollow spherical diameter D, the wall thickness t and the steel pipe diameter d, the wall thickness δ on the distribution pattern of residual stress in the joints, 9 sets of specimens are designed on the basis of Orthogonal experimental design method and the specification of *Technical specification for space frame structures* for the numerical simulation and experimental research. The specific geometric configuration dimensions of samples are demonstrated in the Table 1.

Table 1
Geometric configuration dimension table of samples

Sample Number	Geometric Configuration Dimensions of Samples			
	D / mm	t / mm	d / mm	δ / mm
FEA1	280	8	89	6
FEA2	300	8	89	6
FEA3	300	8	114	6
FEA4	300	8	140	6
FEA5	300	10	114	6
FEA6	300	12	114	6
FEA7	300	12	114	8
FEA8	300	12	114	10
FEA9	350	8	89	6

3. Numerical models and analytical methods

3.1. Numerical models

In order to improve the computational efficiency, the 1/2 model of sphere-pipe weld connection joint has been established according to the symmetry of the hollow spherical joint. The geometric structure of the joint can be seen in Fig. 1. In order to investigate the influence scope of welding temperature on the steel pipe and eliminate the influence of steel pipe end restraint, 1.5 d is selected for the length of steel pipe to establish the finite element model of ANSYS. In order to ensure the calculation accuracy, the division method of mapped meshing is chosen to achieve the discretization of finite element model. A total of 19683 finite elements and 32344 joints have been divided, and the dimension of each element is less than 1/10 of the model dimension except for the wall thickness direction.

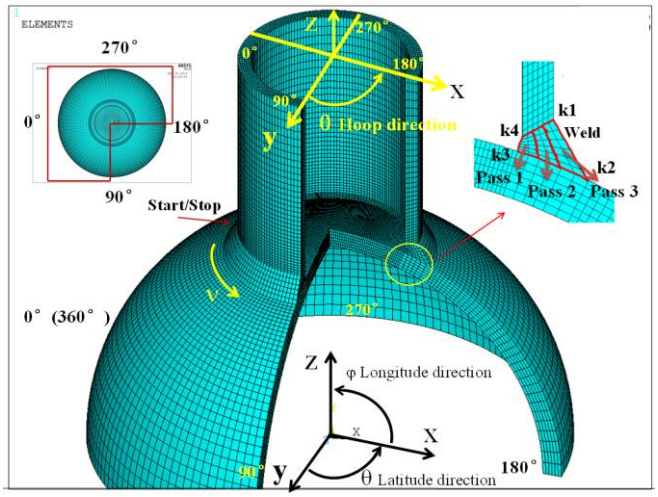

Fig. 1 Schematic diagram of calculation model of the sphere-pipe weld connection joint

3.2. Thermal-structural indirect coupling numerical simulation analytical method

The welding process of the welded hollow spherical joints includes the coupling effects of many physical processes such as heat, force and material phase-change, etc. With the analytical function of thermal-structural coupling of ANSYS, the tracking analysis for temperature field of welds and their heat-affected zone in the welding process can be conducted, and the temperature field can also be precisely adopted on the structural models to obtain the uneven temperature effects after welding. To achieve thermal-structural coupling analysis, all elements will be defined as SOLID70 in the thermal analysis during the welding simulation, and then they will be converted into SOLID185 in the analysis of structural stress. It is assumed that both the welding material and the base material are made of Q235 with the same properties. The material properties are defined according to the curve of material properties changing with temperature [29]. Specifically, several characteristic temperature such as 25°C, 100°C, 200°C, 300°C, 400°C, 500°C, 600°C, 700°C, 750°C, 800°C, 850°C, 900°C, 950°C, 1000°C, 1100°C, 1200°C, 1420°C and 1460°C were selected according to the distribution of the curve. Since the selected characteristic temperature are close to each other, the material properties between adjacent temperature are close to linear changes, the linear interpolation method is used to calculate the temperature and material properties between adjacent temperature in finite element. Due to the large number of temperature points, only the properties of the material at partial temperature are listed in Table 2.

Table 2
Table of the material properties changes with the welding temperature

Temperature/°C	20	250	500	750	1000	1500	1700	2500
Thermal Conductivity/[W/(m·°C)]	50	47	40	27	30	35	45	50
Density/$\times10^3$kg/m^3	7.82	7.70	7.61	7.55	7.490	7.35	7.30	7.09
Specific Heat Capacity/$\times10^2$J/(kg·°C)	4.6	4.8	5.3	6.8	6.7	6.6	7.8	8.2
Poisson's ratio	0.28	0.29	0.31	0.35	0.4	0.49	0.5	0.5
Linear Expansion Coefficient /$\times10^{-5}$m·°C	1.1	1.22	1.39	1.48	1.34	1.33	1.32	1.31
Elastic Modulus /$\times10^6$Pa	205000	187000	150000	70000	20000	0.002	0.0015	0.001
Yield Strength/$\times10^6$Pa	220	175	80	40	10	0.1	-	-

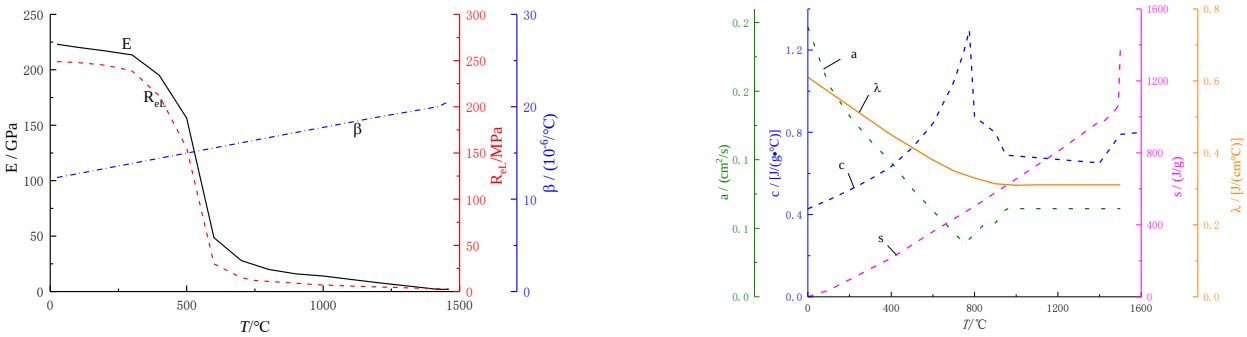

Fig. 2 Curve of material properties changing with temperature

For the boundary conditions of the model, the initial temperature and the room-temperature are set as 25℃ in the thermodynamic analysis; the symmetric planes of the model and the end faces of the steel pipe are the adiabatic plane, the others are set as convective heat transfer surfaces, and the convective heat transfer coefficient is taken as 30J/(m^2•s•℃). In the structural mechanics analysis, symmetric constraints are imposed on the symmetric planes of the hollow sphere.

In order to simulate the manual arc welding used in sphere-pipe welding, the heat generation rate heat source model shown in formula (1) is used. According to the practice of on-site construction, the arc voltage U=15V, the welding current I=160A, and the welding speed v=5mm/s, and the welding thermal efficiency K=0.7. The sphere-pipe butt welds are divided into 3 layers, and the layer of welding beads is numbered from the inside to the outside (See Fig. 1)). Each layer is divided into 80 equal parts in the circumferential direction, and each single element functions as a heat generator.

$$HENG = \frac{K \cdot U \cdot I}{A_i \cdot D \cdot T_i \cdot y} \tag{1}$$

among them, $DT_i = \frac{L_i}{80}$

In this formula, Ai is the cross-sectional area of the welds of each layer; DTi is the welding time of each element, L_i is the length of the welds of each layer; i=1, 2, 3.

Element “birth and death” technology is used to simulate weld formation during welding, as well as localized heating. The specific process is as follows: At the initial moment, all weld elements are set to the "dead" state; Then from the starting point of welding, each weld element is activated one by one from the first layer to the third layer. When a weld element is activated, the welding heat source is moved by applying a heat generation rate to the element, and removing the heat generation rate load from the previous activated element.

There are 240 load steps in the welding process, with a total duration of (80×ΣDT_i). After all weld elements are activated, the cooling phase of the weld comes. In the cooling stage, the model exchanges heat with the outside until the whole model returns to room-temperature of 25°C. The cooling time of 80 minutes in total is divided into 20 load steps with a step length of 240 s; The heat generation rate of the last weld element is removed in the first cooling load step. So far, the thermodynamic analysis of the sphere-pipe connection weld in the welding process is completed, then the model elements will be converted into mechanical analysis elements, and a symmetric constraint is applied on the symmetric plane of the hollow sphere for mechanical analysis.

4. Analysis of temperature field change law during welding

The uneven temperature rises and fall in the welding process is the main cause of welding residual stress. Therefore, clarifying the temperature field change law of welds and their heat-affected zone during welding can qualitatively test the accuracy and effectiveness of the subsequent simulation of the sphere-pipe welding process. Due to space limitation, sample FEA7 is taken as an example to track the 3-layer welding process of the sphere-pipe single butt seam and analyze its temperature field.

4.1. Nephograms of temperature field distribution

During the welding of sphere-pipe welds, the welding heat source moves counterclockwise from the position of 0° on the weld bead, then passes through 90°, 180°, 270° and 360°, and circulates 3 times in turn. The temperature field distribution nephograms of the FEA7 model at the moment when the welding heat source of the first layer of weld passes through 90° and that of the third layer of weld passes through 270° are extracted respectively, as shown in Fig. 3. It can be seen from Fig. 3 that the highest temperature is in the molten pool during welding, and gradually spreads to the rest of the joints with the progress of welding. The temperature distribution presents a crescent shape, and the temperature gradient gradually increases along the welding direction, which conforms to the characteristics of local instantaneous high temperature of welds during welding. After cooling, the overall temperature of the model is restored to room-temperature of 25°C.

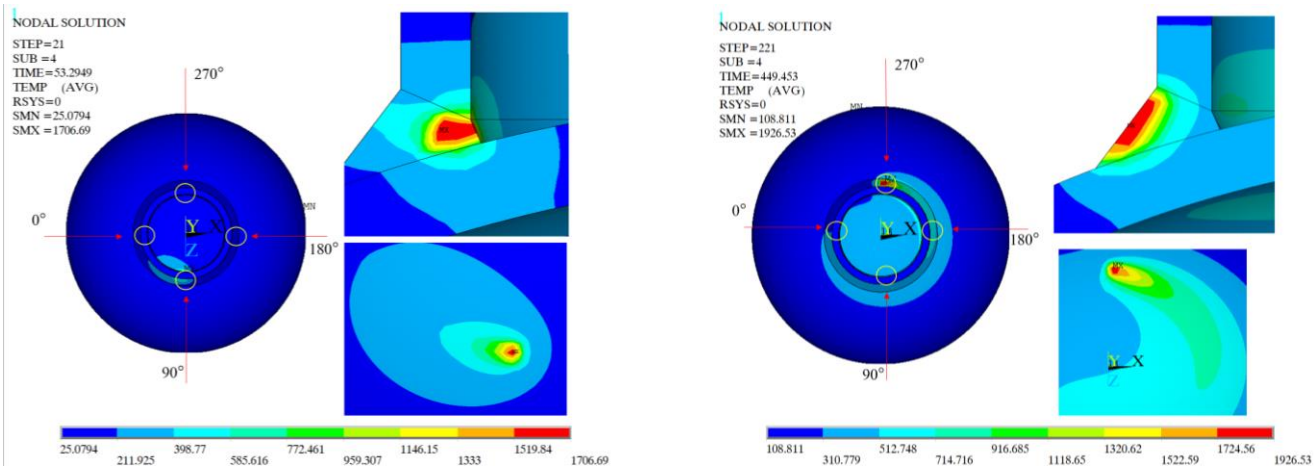

(a) Welding through 90° (b) Welding through 270°

Fig. 3 Temperature distribution nephograms of hollow spherical joints during welding (Unit: °C)

4.2. Variation law of temperature of key weld joints with welding process

In order to more intuitively observe the variation of local temperature of welds with time in the welding process more intuitively, the temperature variation curve of key points at the position of welds is drawn, as shown in Fig. 4. Four points on the initial welding section that can be in direct contact with the heat source are selected as key points (See Fig. 1). The key points 4 and 3 are in direct contact with the heat source during the welding of the first layer, while the key points 1 and 2 are in direct contact with the heat source during the welding of the third layer. It can be seen from Fig. 4 that each key point has undergone 3 heating processes, which directly reflects that the weld has gone through the process of 3 layers of welding. Key points 3 and 4 reach temperature extremes during welding at the first layer, while key points 1 and 2 reach temperature extremes during welding at the third layer, which conforms to the welding sequence from inside to outside. When the key points are in direct contact with the heat source, their temperature exceeds the melting point of the steel (usually 1538°C). And after cooling, the temperature of each key point returns to room-temperature.

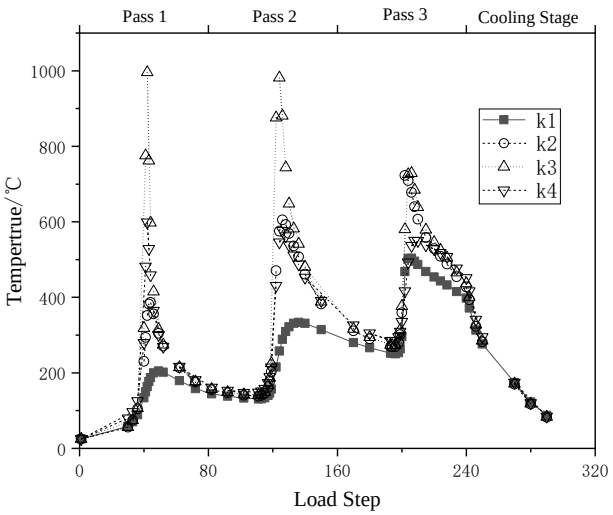

Fig. 4 Temperature variation curve of key points

Based on the temperature characteristics of the above finite element model, it can be seen that the finite element model established in this paper can effectively simulate the sphere-pipe welding process of hollow spherical joints, and then it can be considered that the residual stress of the joints after the completion of cooling can be regarded as the welding residual stress.

5. Calculation results of welding residual stress in different directions

Since the temperature field in the welding process presents three-dimensional characteristics in the joints, the welding residual stress in the joints also presents three-dimensional characteristics. According to the analysis, it is found that the geometric configuration dimension of the joints will affect the numerical value of the welding residual stress, but will not have a great impact on its distribution law. Therefore, the FEA7 model is still taken as an example to introduce the distribution law of the welding residual stress of sphere-pipe connection welds of the welded hollow spherical joints.

5.1. Distribution nephograms of welding residual stress in different directions

According to the coordinate system established in Fig. 1, the residual stress nephogram in each direction after welding are drawn (See Fig. 5). It can be seen from Fig. 5 that the residual stress in each direction is mainly distributed near the welds, and is relatively uniform along the circumferential direction of the steel pipe.

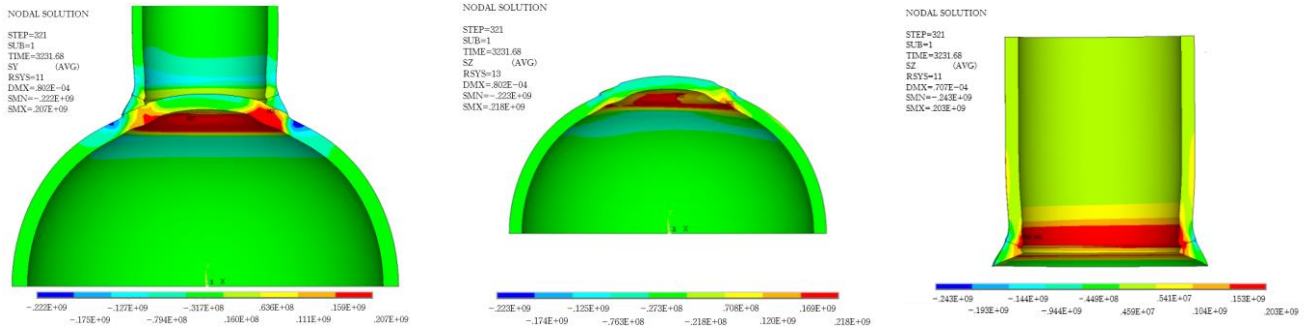

(a) Circumferential residual stress σ_θ (b) Longitudinal residual stress σ_φ (c) Axial residual stress σ_z

Fig. 5 Welding residual stress nephograms (Unit: Pa)

It can be seen from Fig.5-a) that the shrinkage of the welds along the length direction leads to the corresponding necking of the steel pipe and hollow sphere on both sides of the welds, which can partially release the circumferential residual stress. Moreover, due to the relatively weak constraint of the steel pipe, the necking of the steel pipe is more obvious than that of the hollow sphere. Therefore, the circumferential residual stress σ_θ on the hollow sphere is generally greater than that of the steel pipe. In addition, the area directly in contact with the weld on the hollow ball, the heat dissipation condition is the worst, welding weld heat will be directly into this area. However, the heat will be finally cooled after the heat dissipation of the welds during cooling, so it will be constrained by the outer surface that is cooled first, resulting in the stress in this area being tensile on the inner surface and compressed on the outer surface. The maximum circumferential residual compressive stress is -222MPa at a certain distance from the outer surface of the hollow sphere to the weld toes, and the maximum circumferential residual tensile stress is 207MPa inside the hollow sphere under the welds.

As can be seen from Fig. 5-b) and Fig. 5-c), the necking of steel pipe and hollow sphere is also caused by the shrinkage of welds along the direction of length, so that the steel pipe and hollow sphere near the welds show obvious bending characteristics along the wall thickness direction respectively. Therefore, near the welds, the longitude residual tensile stress of the hollow sphere and the axial residual tensile stress of the steel pipe are distributed in their inner areas, with the maximum values of 218 MPa and 203 MPa respectively; the longitude residual compressive stress of the hollow sphere and the axial residual compressive stress of the steel pipe are distributed in the outer area, with the maximum values of -223 MPa and -243 MPa respectively at the weld toes. In the outer area of welds, the residual stress values of the steel pipe and the hollow sphere in the thickness direction are relatively low, which are less than 30MPa except at the weld junctions.

5.2. Distribution law of welding residual stress in different directions

5.2.1. Distribution law of σ_θ

In order to clarify the distribution law of welding residual stress in hollow spheres, the 180° section of FEA7 model is still selected to analyze the distribution law of residual stress at different wall thickness positions of hollow spheres. Fig. 6 shows the distribution curve of circumferential residual stress σ_θ along the longitudinal direction at different wall thickness positions of the hollow sphere along the longitudinal direction. The angles on the spherical surface corresponding to the weld toe are 18.6° and 26.1° respectively. Hollow sphere is divided into three areas: the inside of the circumferential weld, the weld area in direct contact with the circumferential weld and the outside of the circumferential weld. It can be seen from Fig. 6 that the tensile stress is mainly concentrated in the weld and adjacent areas, while the compressive stress is concentrated in the outside of the weld.

The distribution laws of σ_θ along the longitudinal direction at different wall thickness positions of the hollow sphere are similar along the longitudinal direction. The tensile stress in the weld area gradually decreases towards the inside and outside of the circumferential weld, and then develops to the compressive stress direction until a critical position and then to the tensile stress direction.

In addition, combined with Fig. 5-a) and Fig. 6, it can be seen that the maximum circumferential residual compressive stress on the hollow spherical surface occurs at the position of φ=5.6° from the outer weld toe in the outer area encircling the weld on the exterior surface of the hollow sphere. The maximum residual tensile stress occurs at the position of φ=20.8° and R=0.144m inside the hollow spherical wall thickness.

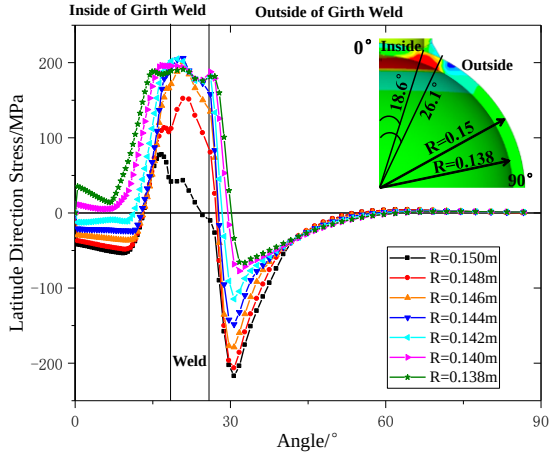

Fig. 6 Distribution curve of σ_θ at different wall thickness

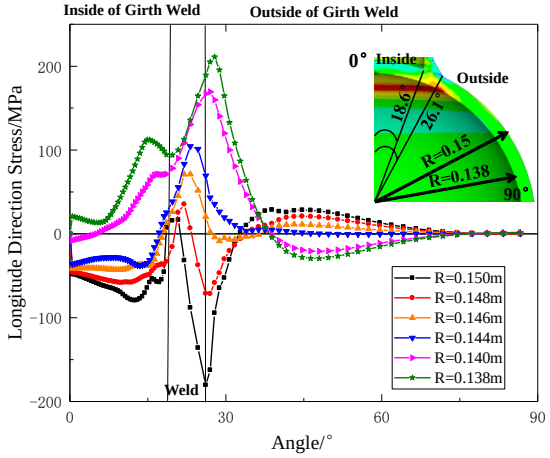

Fig. 7 Distribution curve of σ_φ at different wall thickness

5.2.2. Distribution law of σ_φ

Fig. 7 shows the distribution curve of σ_φ along the longitudinal direction of hollow spheres at different wall thicknesses along the longitudinal direction of hollow spheres. As can be seen that from φ=0°~36°, σ_φ gradually changes from tensile stress to compressive stress from the inner surface to the outer surface of the hollow sphere; from φ=36°~90°, the opposite is true.

Specially, on the outer wall of the hollow sphere(R=0.15m), σ_φ obtains the maximum compressive stress of -180.3 MPa at φ=26.1°, then decreases with the increase of φ and reaches 0 at φ=32.6°; then, with further increase of φ, σ_φ turns into tensile stress and obtains the extreme value of 28.6MPa at φ=38.9°. On the inner wall of the hollow sphere (R=0.138m), σ_φ obtains the maximum tensile stress of 205.1MPa at φ=27°, then gradually decreases with the increase of angle φ. It obtains the same value of 23.1MPa at the outer wall of φ=36.2°, and then reaches 0MPa at 38.4°. As the angle decreases, it turns into compressive stress and obtains an extreme value of 29.4 MPa at φ=48°.

In addition, by comparing σ_θ and σ_φ at the same position of welds, it can also be found that σ_φ is always greater than σ_θ, which indicates that the steel is more likely to yield along the longitudinal direction at the weld, that is, the axial direction of the welded hollow spherical joints, especially for the compressed joints, the superposition of residual compressive stress and external load will lead to the failure of joint extraction. In the range of 15mm~20mm from the weld, σ_θ will reach the peak, which is extremely unfavorable to the bending of joints.

6. Experimental studies and verification of welding residual stress

Although the distribution of residual stress in the welded hollow spherical joints can be obtained comprehensively by numerical simulation, the accuracy and reliability need to be verified because the welding heat source and material phase-changing are properly assumed in the calculation process. Therefore, in order to verify the reliability of the numerical simulation results, two sets of equal-scale samples S-1 and S-2 are designed with reference to the FEA7 model, and the magnetic measurement method is used to test and analyze the welding residual stress on the surface of the hollow sphere. The geometric dimensions and welding process of samples S-1 and S-2 are exactly the same as those of FEA7 model. Specific structural dimensions can be seen in Table 1.

6.1. Basic principle and test overview of magnetic measurement method

The magnetic measurement method is used to measure the initial stress inside steel based on the magneto strictive effect of ferromagnetic materials [30]. In the plane stress state, the current difference output in the principal stress direction and the principal stress difference have a single-value linear relationship shown in Formula (2).

$$(I_1 - I_2) = \alpha(\sigma_1 - \sigma_2) \tag{2}$$

In this formula, σ_1 and σ_2 are the maximum and minimum principal stresses respectively, in MPa; I_1 and I_2 are the current output values in the direction of maximum and minimum principal stresses respectively, in mA; α is the sensitivity coefficient, in mA/MPa.

Since the direction of principal stress is unknown, the direction angle of principal stresses and the differences of principal stresses can be determined by Formula (3) and Formula (4) respectively.

$$\theta = -\frac{1}{2}tan^{-1}\left(\frac{2I_{45}-I_0-I_{90}}{I_{90}-I_0}\right) \tag{3}$$

$$(\sigma_1 - \sigma_2) = \frac{I_{90}-I_0}{a\cos 2\theta} \tag{4}$$

In the above formula, θ is the included angle between σ_1 and the vertical direction of the shaft network; I_0, I_4 and I_{90} are the measured current values in three directions of 0°, 45° and 90° respectively.

After the principal stress difference and direction angle are calculated according to the above formula, the principal stress can be separated by the shear stress difference method, and the stress component of any point P can be calculated according to Formulas (5) ~ (7).

$$(\sigma_x)_P = (\sigma_x)_0 - \int_0^P \frac{\partial \tau_{xy}}{\partial y}dx \tag{5}$$

$$\left(\sigma_y\right)_P = (\sigma_x)_P - (\sigma_1 - \sigma_2)_P \sin 2\theta_P \tag{6}$$

$$\left(\tau_{xy}\right)_P = \frac{(\sigma_1-\sigma_2)_P}{2}\sin 2\theta_P \tag{7}$$

In this formula, $(\sigma_x)_0$ is the known stress value of the boundary point, and the $(\sigma_x)_0$ of the free boundary is set as 0. In calculation, increment is used to replace differentiation.

When the magnetic measurement method is used, after the samples are welded and cooled to room-temperature, an auxiliary grid is established at the measuring point on the surface of the hollow sphere, and the measuring points are represented by square grid joints and numbered, as shown in Fig. 8. The coordinate system corresponds to the spherical coordinate system shown in Fig. 1.

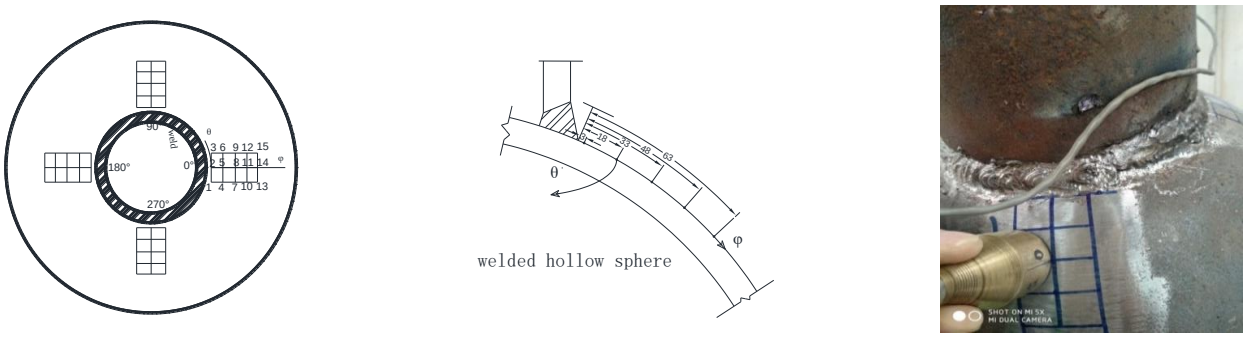

(a) Vertical view (b) Section (c) Real picture

Fig. 8 Layout of residual stress measuring points

In order to be representative, a test area is set every 90° along the circumferential direction from the welding starting point. Five measuring points are evenly arranged along the longitudinal direction in each measuring area, and three measuring points are arranged along the circumferential direction. During measurement, the average value of the three measuring points in the circumferential direction is taken as the stress value of the longitude position. SC21B three-dimensional stress distribution magnetic instrument is used for measurement. The measuring instrument and process are shown in Fig. 9.

Fig. 9 Measurement process of residual stress

6.2. Comparative analysis of test results and numerical simulation results

σ_θ and σ_φ of samples S-1 and S-2 at measuring points can be measured by magnetic measurement method, and compared with the finite element calculation results in Section 5.1, as shown in Figs. 10 and 11.

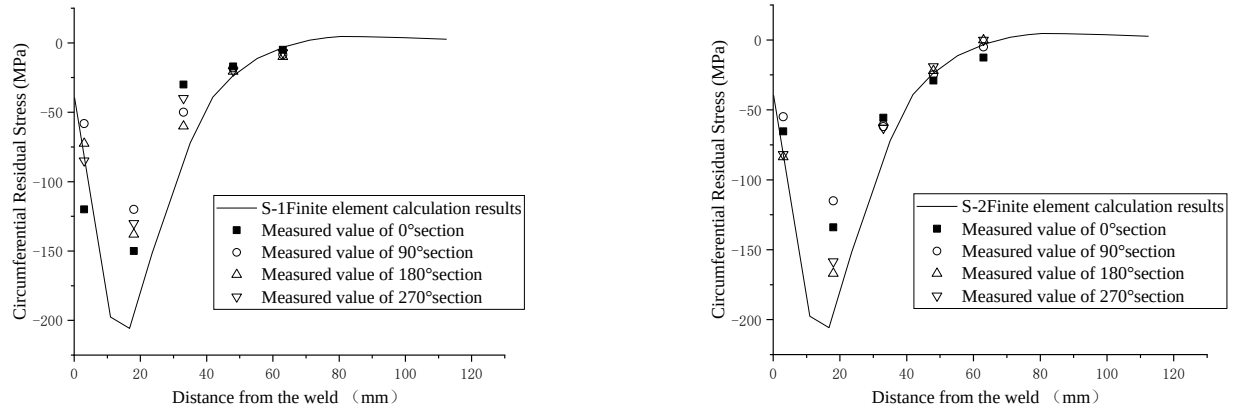

(a) S-1 (b) S-2

Fig. 10 Comparison of σ_θ by testing and finite element calculation

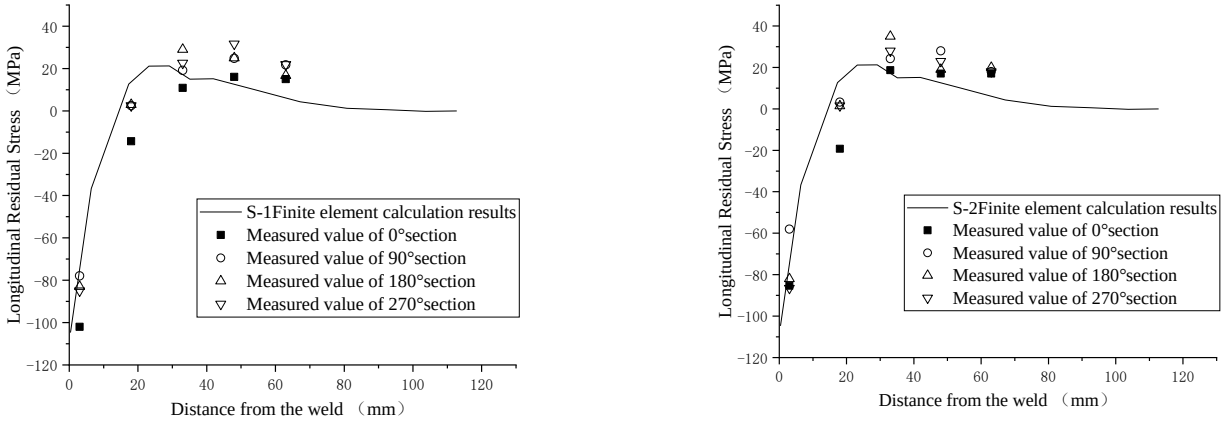

(a) S-1 (b) S-2

Fig. 11 Comparison of σ_φ by testing and finite element calculation

It can be seen from Fig. 10 and Fig. 11 that the distribution law and change trend of welding residual stress of samples S-1 and S-2 are in good agreement with the finite element calculation results of FEA7.

It can be seen in Fig. 10 that the σ_θ of samples S-1 and S-2 increases gradually from weld toe and reaches peak value at the measuring point that is 18mm away from weld. This value is 6.44% and 7.83% different from the finite element calculation respectively, which indicates that the test results are in good agreement with the finite element calculation results. Specifically, the maximum σ_θ of sample S-1 is -150MPa, 27.4% smaller than the peak value calculated through the finite element method; of sample S-2, the value of maximum σ_θ is -167MPa, 17.73% smaller than that than the peak value calculated through the finite element method.

It can also be seen from Fig. 11 that for samples S-1 and S-2, the maximum σ_φ is reached at the weld toe and decreases with the distance from the weld growing, which is the same as the result through the finite element calculation. Specifically, the maximum σ_φ of sample S-1 is -102MPa, which is only 2.86% smaller than the value by the method of finite element calculation. The maximum σ_φ of sample S-2, the maximum is -85.7MPa, which is 30.6% smaller than that through the finite element method.

From the analysis above, the finite element calculation results of FEA7 are always larger than the test values of S-1 and S-2. it is known that for FEA7, the result by the method of finite element calculation is always larger than the testing value of samples S-1 and S-2. As for reasons for this conclusion, on the one hand, it is difficult to measure the peak value of an accurate point because the magnetic measurement method measures the average stress at the probe; on the other hand, the actual result is the stress at the center of the probe. For the 3cm range (probe diameter) close to the weld, the probe is hard to reach due to the obstruction of steel pipe forming a dead angle. However, the similarity between the changing trends of the test results and the finite element calculation results can still verify the reliability of the above-mentioned numerical model to a certain extent.

7. Calculation result of Von Mises equivalent welding residual stress

From the analysis above, it can be seen that the residual stress of the welded hollow spherical weld and its heat-affected zone is in complex stress condition. The unidirectional stress state is difficult to describe the actual working state, so it is necessary to extract the equivalent stress that can characterize the complex stress state according to actual yield criterion.

7.1. Nephograms of Von Mises equivalent welding residual stress distribution

By comparing the test result and finite element result, it is known that the meticulously-organized numerical model is reliable to some extent. Therefore, the Von Mises equivalent stress nephographs of the joint (See Fig. 12) is extracted from the FEA1 model as an example to analyze its complex stress state. It can be seen from Fig. 12-a) that the extreme value of Von Mises equivalent residual stress at joints has reached 220MPa, which is close to the yield strength of the material. Hence, the weld and its adjacent area will become the weak areas. With the distance from the weld growing, the welding residual stress gradually decreases until it dissipates, which conforms to the physical law in Fig. 3 that the temperature and temperature gradient decrease as the distance from the weld grows. The smaller the temperature gradient is, the smaller local constraint is, and the stress is smaller. In addition, it can be seen from Fig. 12-a) that in the area near the weld, along the circumferential direction of the steel pipe, the welding residual stress is basically at the same level except for the starting point of welding. While the residual stress at the welding start and its adjacent areas is obvious difference. The reason for this difference is that the weld is a circular closed weld, and the start of welding is both the arcing point and the stopping point of arc welding. Each layer experiences two instantaneous high temperatures, resulting in complex and irregular stress in this area.

7.1.1. Calculation results of welding residual stress in steel pipe

According to Fig. 12-b), the maximum Von Mises equivalent stress of steel pipe, 216MPa, is in the direct contact between the pipe and the weld. From the stress distribution on the section, along the direction of thickness, the welding residual stress at the inner and outer boundaries is larger than the internal stress of the steel pipe, showing a pattern that is high on both sides and low inside. At the same horizontal height of the steel pipe, the stress value is basically the same. The minimum stress of the steel pipe is 1.19MPa, so the stress on the pipe can be ignored after a certain distance from the weld, which indicates that the influence area of welding on the steel pipe has a certain range.

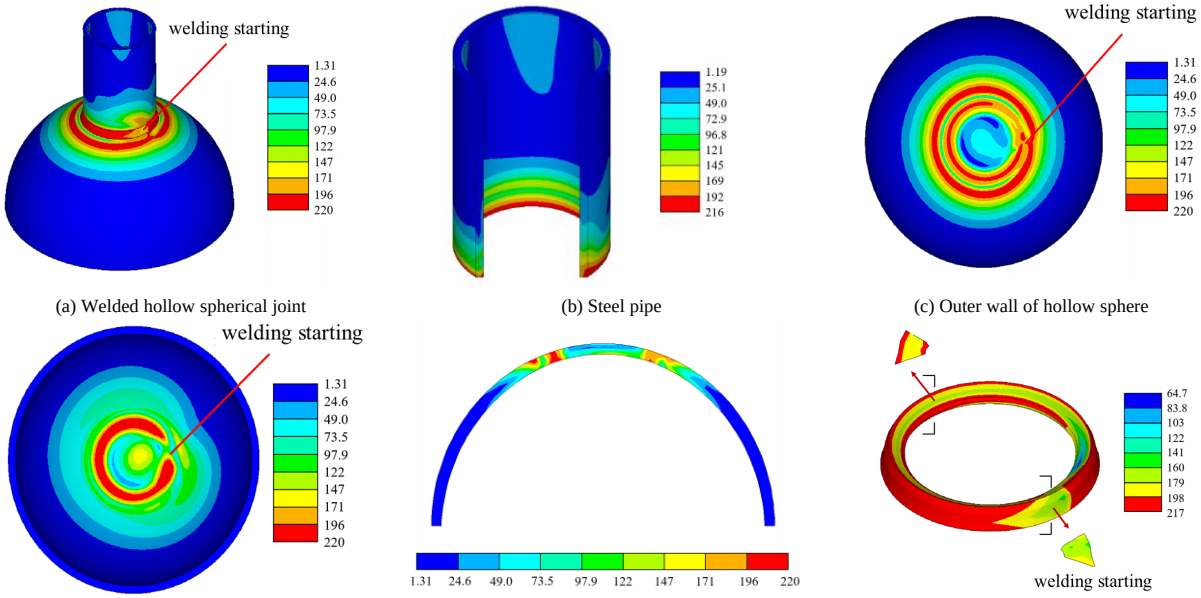

(a) Welded hollow spherical joint (b) Steel pipe (c) Outer wall of hollow sphere

(d) Inner wall of hollow sphere (e) Section of welding start (f) Weld

Fig. 12 Nephograms of welding residual stress of welded hollow spherical joint (Unit: MPa).

7.1.2. Calculation results of welding residual stress in hollow sphere

It can be seen from Fig. 12-c) and Fig. 12-d) that the maximum welding residual stress in the hollow sphere is 220MPa and the minimum is 1.31MPa. The difference between the welding residual stress at the starting position of welding and the stress at other positions at the same latitude is more obvious on the hollow sphere.

Similarly, there is also a certain welding influence area on the hollow sphere, which is similar to the stress distribution on steel pipe. Beyond this area, the welding residual stress can be ignored; moreover, the welding residual stress on the outer wall of the hollow sphere in contact with air is larger than that on the inner wall. The welding residual stress along the direction of thickness is also high on both sides and low inside.

It is worth mentioning that the maximum welding residual stress on the inner wall of the hollow sphere appears below the corresponding position of the weld, while the maximum of the outer wall appears on both sides of the direct contact of the weld. This proves that thermal boundary condition has an influence on the welding residual stress of joints, and the residual stress on a boundary has a larger value. That is, the boundary condition is the reason for the distribution of welding residual stress in the thickness direction of "high on both sides and low inside" and the difference of stress distribution on the inner and outer walls of the hollow sphere.

7.1.3. Calculation results of welding residual stress in weld

It can be seen from Fig. 12-f) that the welding residual stress of sphere-pipe weld is relatively large, with the maximum of 217MPa and minimum of 64.7MPa. Similarly, the stress on the boundary in contact with air is larger than that in the interior not in contact with air. Except for the start of welding, the distribution of stress on the weld is approximately similar. Generally, in the process of welding, a heat-affected zone is formed at the hollow spherical joint. Within this zone, the closer to the weld, the larger the residual stress is, and the influence of welding outside this zone can be ignored. Since the start of welding experiences one more heating than the other positions on the same circumference, the residual stress here is different from that of the other positions.

7.2. Distribution pattern of the welding residual stress

To make clear the specific zone influenced range of welding residual stress, a simplified distribution mode of welding residual stress based on Von Mises yield criterion is concluded according to the above calculation results. It is assumed that the welding residual stress along the direction of thickness remains unchanged, and the resultant stress along the direction is taken as the welding residual stress at this position. To this end, nine paths are established on the same circumference as the welded hollow spherical joint (See Fig. 13). The paths are selected according to the interval of element division. Within the weld， paths are separated by one element, while the others by two elements.

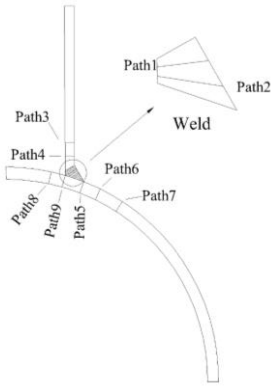

Fig. 13 Schematic diagram of the description paths of welding residual stress on the section

According to the above method, the welding residual stress distribution curve of the 9 paths shown in Fig. 13 are drawn (See Fig. 14). The curves adopt polar coordinate system, and the angle of the start of welding is set to 0°. The circumference is specified as the zero- stress point. The closer to the center of the circle, the greater the stress value.

It is clear that welds and areas adjacent to them on the hollow sphere have relatively larger residual stress by comparing the welding residual stress distribution curves of each path. Meanwhile, combined with the nephograms of stress in Fig. 12, it is obvious that the repeated temperature rise and fall at the start of welding has a great impact on the distribution of welding residual stress in this area. Specifically, the repeated heating rise at the starting position has the largest impact on the steel pipe, resulting in the largest stress fluctuation area on Path3 (Fig. 14-c)) and Path4 (Fig.14-d)), at about -45°~45°. The second largest is on Path1 (Fig. 14-a)) and Path2 (Fig. 14-b)) in the weld, with a region of -13.5 ° ~45 °; And the paths on the hollow sphere have the smallest, about -18 ° ~18 °.

On the other hand, in terms of specific fluctuation range, the variation rules of each region are also different: the fluctuation amplitude of Path1 and Path2 in the weld is the largest, while the fluctuation amplitude of the paths on the steel pipe and hollow sphere is relatively small. The reason may be that the direct contact between the weld and the high-temperature heat source is instantaneous, while influence on the steel pipe and hollow sphere is continuous because the propagation of temperature needs a certain time. Moreover, from the stress distribution curves of each path, it is also apparent that the extreme value of stress is not at the starting position of welding since when the start experiences high temperature again, the weld there melts again, and the weld areas generated already are no longer constrained by the material there. As a result, the welding residual stress in the adjacent areas will be partially released, and dips shown in Fig. 14 appear on the stress curves.

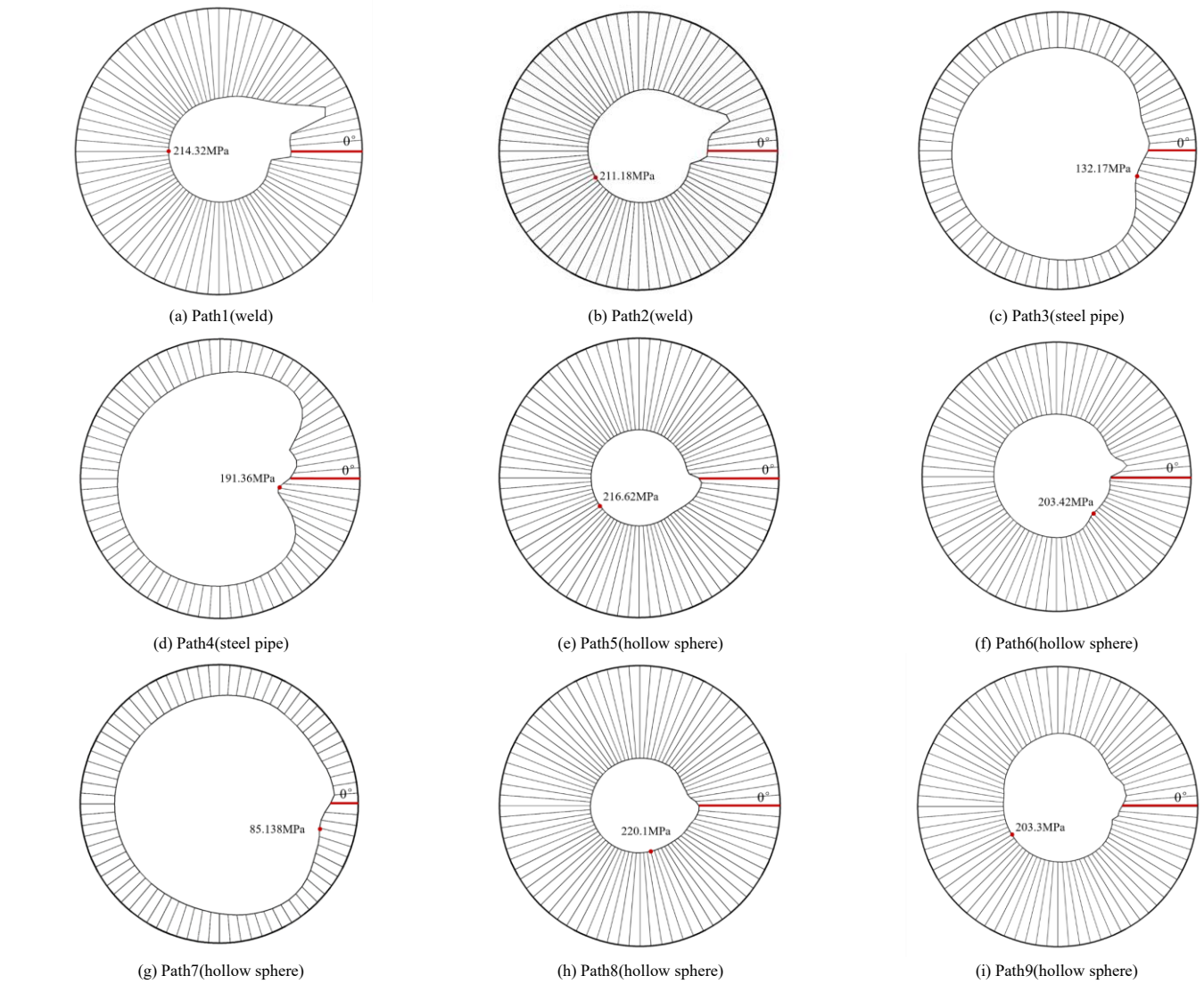

Fig. 14 Curves of welding residual stress distribution of the paths.

7.3. Determination of the welding heat-affected zone

Fig. 14 actually shows the stress distribution curve of the weld and its surrounding area along the circumferential direction. In engineering practice, more attention is paid to the stress distribution pattern along the vertical section. From Fig. 14, we can also notice a significant feature of the circumferential distribution of stress, that is, for the same circumferential path, except the start of welding, the stress distribution curves of other positions except the start of welding, are close to a concentric circle, and their stress values are almost equal. Therefore, combined with the good plastic characteristics of steel, it can be assumed that the stress of the paths in Fig. 14 is completely evenly distributed along the circumferential direction. A fixed stress value is taken along the circumference to ensures that the value ensures that the resultant force along the circumference is equal to the actual stress. Taking Path1 as an example, its stress curve is drawn through the Cartesian coordinate system, and then its simplified stress value is obtained based on the basis that the areas formed by the curve and the x-axis are equal in dimension (See Fig. 15). Hence, a simplified distribution model is obtained. It shows the welding residual stress on the section of hollow spherical joint according to Von Mises yield criterion (See Fig. 16).

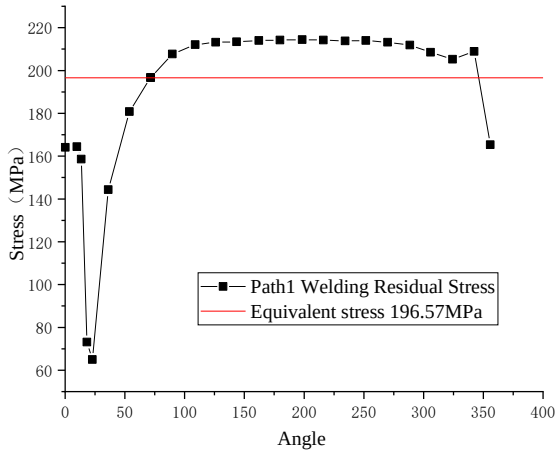

Fig. 15 Example of the simplified method for welding residual stress on the same circumference

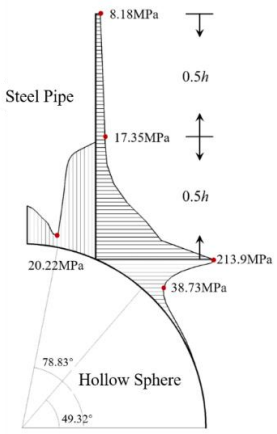

Fig.16 Simplified distribution pattern of welding residual stress on spherical section

It is known from Fig. 16 that on the vertical section of joints, the maximum welding residual stress is 213.9MPa, which is only 6.1MPa different from the accurate value of 220MPa by the method of finite element calculation in Section 7.1. The difference is within the acceptable range; and the variation law of residual stress is completely consistent with the analytical results in Section 6.1, that is, the residual stress decreases as the distance from the weld grows. Therefore, the more obvious Fig. 16 can be used to analyze the heat-affected zone of joints.

Specifically, at the 1/2 height of the steel pipe in Fig. 16, the welding residual stress reduces to 17.35MPa, 91.89% lower than the peak stress; at the latitude φ=49.32° on the hollow sphere, the residual stress decreases to 38.73MPa, 81.89% lower than the peak. The stress has reduced to a relatively small value. If 5% of the yield strength of the material is taken as the basis of whether the welding residual stress can be ignored to judge the stress influence area of welding. The welding influence area of each finite element model is shown in Fig. 17.

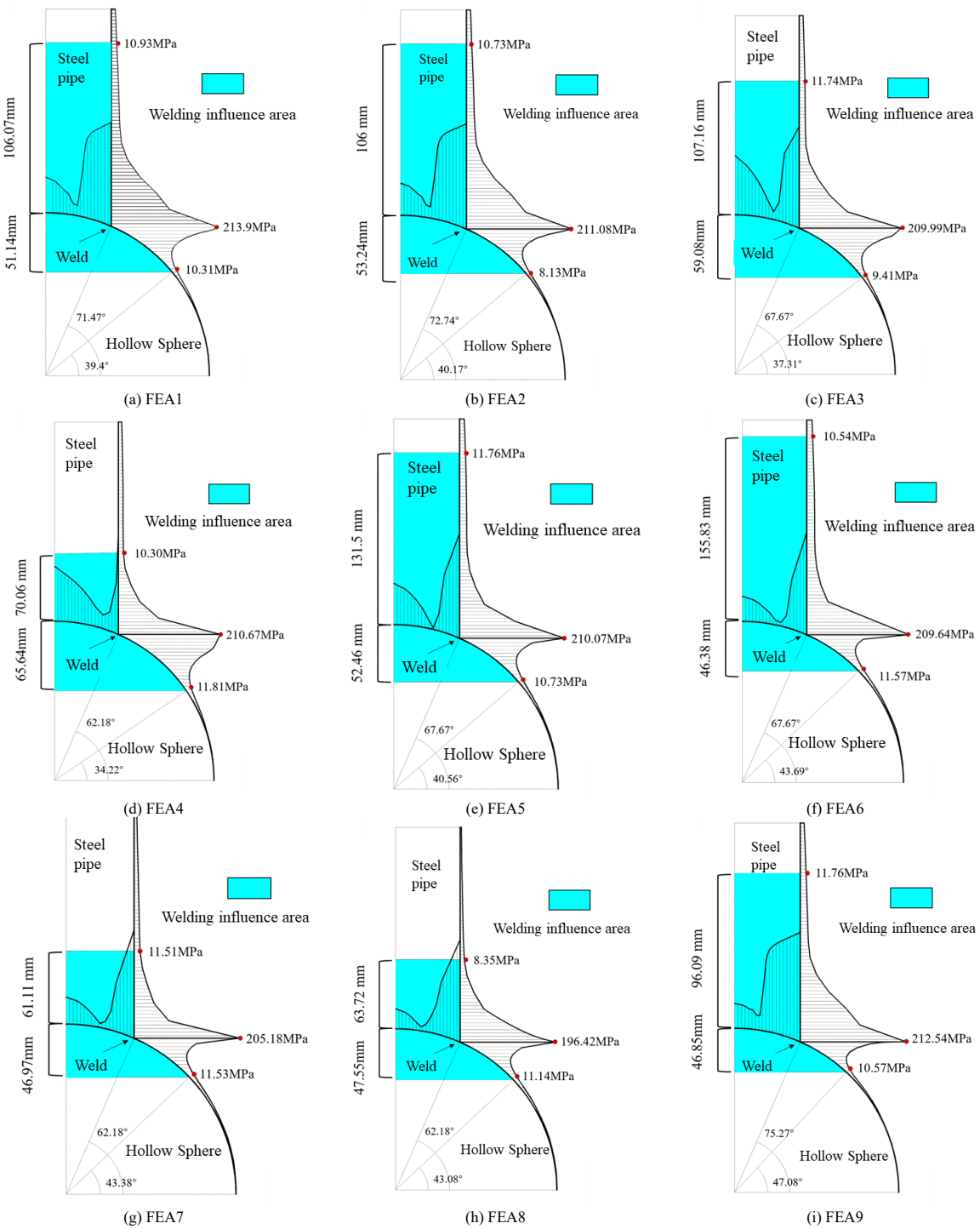

Fig. 17 Simplified distribution model of welding residual stress of the sections of the models

By comparing the models in Fig. 17, it can be seen that the distribution law of welding residual stress in each model is exactly the same, indicating that this kind of hollow spherical joint has the same distribution pattern of welding residual stress. The dimension of hollow spherical joint doesn't have a big impact on the maximum welding residual stress. The maximum of each model is about 210MPa, but it will affect the range of welding influence zone.

7.4. Effects of configuration dimension of joint on welding heat-affected zone

To more clearly analyze the influence law of each parameter of dimension on the welding influence zone, the trend charts that show the variation of the maximum welding residual stress of the joint and the proportion of the welding influence zone on the steel pipe and hollow sphere as a single parameter varies are drawn (See Fig. 18). Among them, the proportion of the influence area on the steel pipe is the ratio of the length of the influence area on the steel pipe to the total length of the pipe, and the proportion of the influence area on the hollow sphere is the ratio of the central angle of the influence area on the 1/4 arc section of the hollow sphere to 90 °.

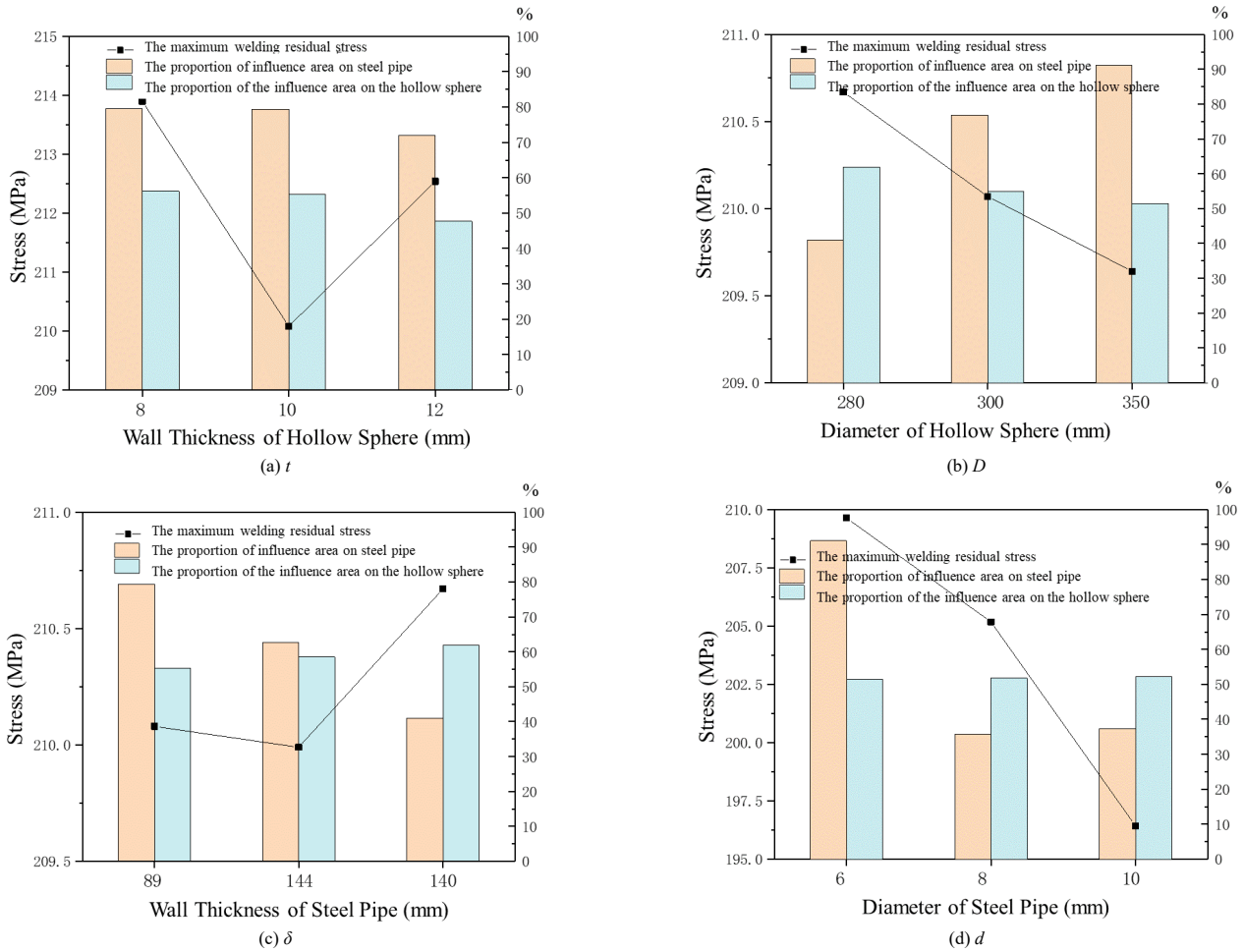

Fig. 18 Effects of dimension parameter on welding residual stress on joints

According to Fig. 18, the wall thickness of steel pipe δ has the greatest effect on the maximum welding residual stress. When the thickness increases, the maximum residual stress decreases; In addition, the maximum also falls with the increase of the diameter of the hollow sphere D, but compared with the wall thickness of steel pipe t, the reduction is very small. The influence of steel pipe diameter d and hollow sphere wall thickness t on the welding residual stress is characterized as the pattern of "V", which means there is an optimal dimension to minimize the welding residual stress of the whole joint.

Comparing the influence areas of welding residual stress of different configuration dimensions in Fig. 18, it is not difficult to find that in general, when the configuration dimensions of joints change, the influence areas on the hollow sphere change a little. It can be seen from Fig. 18-a) and 18-b) that with the increase of t and D, the influence areas on the hollow sphere decrease slightly, and the influence areas on the steel pipe also have some change larger than those on the sphere; from Fig. 18-c) and 18-d) it is known that as δ and d increase, the influence areas on the pipe decrease gradually, while those on the hollow sphere change a little. Reasons for these rules are that the dimension of weld is jointly determined by δ, d, and D. On the one hand, the larger δ is, the wider the weld is, and a large section of weld may make transition of the sections at welds tend to be smooth, which can reduce stress concentration at the weld so as to reduce the maximum welding residual stress and the range of influence zone on the steel pipe to some extent; on the other hand, the larger d is, the longer the weld is, but meanwhile, growing surface area in contact with the weld makes larger the heat dissipation area on the weld. Therefore, the influence area on the pipe may be reduced. Similarly, the contact area between the weld and the hollow sphere increases with the rise of D, which will also make transition of the sections of welds tend to be smooth. Moreover, this will also enlarge the heat dissipation area and reduce the influence area of the hollow sphere.

Specifically, the influence area on the steel pipe of FEA7 model is the smallest, at 35.74%. The largest, 91.13%, is on FEA6 model. Thus, the influence area on the steel pipe is 0.6d~1.35d from the weld. The model with the smallest proportion of influence area on the hollow sphere is FEA9, with an influence area of 47.69%, and the largest is 61.98% on FEA4. In the direction vertical to the weld, the influence area is roughly 0.5d from the weld, the range of change is smaller than that of the steel pipe.

8. Conclusions

The residual stress in the directions is mainly distributed near the circumferential weld. The maximum residual stress on the steel pipe is the axial residual stress of 243MPa and that on the hollow sphere is the longitudinal residual stress of 223MPa. Through the analysis, the circumferential residual stress along the longitude of the sphere was converted from a tensile stress to a compressive stress. After reached the extreme value, the residual stress gradually reduced. And the axial residual stress reached the extreme value at the weld and then gradually dissipated as away from the weld. Except for the start position of welding of repeated temperature rise and fall, stress values are almost the same; therefore, in integral analysis of the structure, it can be assumed that stress is completely evenly distributed along the circumferential direction, which means a fixed stress can be taken along the circumference to ensure that the resultant force along the circumference is equal to that of the actual stress.

The longitudinal residual stress at the same position of welds is always larger than the circumferential residual stress, indicating that steel is easier to yield along the longitudinal direction at the weld. Therefore, the superposition of residual compressive stress and external load is easier to cause the compression joint failure; however, in the range of 15mm~20mm from the weld, the circumferential residual stress will reach the peak, which is extremely unfavorable to the bending of the joint.

The influence of the geometric dimension of welded hollow spherical joints on the welding residual stress of joints is complex. The influence area on the steel pipe is about 0.6d~1.35d from the weld, and the area on the sphere is about 0.5d from the weld; When the wall thickness of steel pipe δ or the diameter of hollow sphere D increases, the maximum welding residual stress decreases. The influence of steel pipe diameter d and hollow sphere wall thickness t on the welding residual stress is characterized as the pattern of V, which means there is an optimal dimension to minimize the welding residual stress of the whole joint. The research found, the dimension parameter of the joint mainly affects the range of the welding influence zone on the joint, and the extreme value of welding residual stress is not affected much.

Funding acknowledgments

This work was supported by 2022 Technology Innovation and Application 531 Development Project of Nanan District, Chongqing (2022), and the Projects of Postgraduate Research Innovation in Chongqing(2020S0007).

Reference

[1] Zhongwei Zhao, Hongwei Zhang, Lina Xian, Haiqing Liu. Tensile strength of Q345 steel with random pitting corrosion based on numerical analysis. Thin-Walled Structures. 2020;148, 106579.

[2] ZHANG Yanhua. Principles of Welding Mechanics and Structural Integrity. Architecture & Building Press. 2007; China: Beijing.

[3] Farajian, M. Welding residual stress behavior under mechanical loading. Welding in the World. 2013; 57 (2), 157-169.

[4] Osgood W F. Mechanics[M]. Crawford: Crawford Press, 2007.

[5] Brar, G. S., and Singh, C. S. Fea of residual stress in cruciform welded joint of hollow sectional tubes. Journal of Constructional Steel Research. 2014;102, 44-58.

[6] W. Y. Wang, G. Q. Li, Y. Ge. Residual Stress Study on Welded Section of High Strength Q460 Steel After Fire Exposure. Advanced Steel Construction. 2015;11(2), 150-164.

[7] Bo Yang, Shidong Nie, Shao-Bo Kang, Gang Xiong, Ying Hu, Jubo Bai, Weifu Zhang, Guoxin Dai. Residual Stress Measurement on Welded Q345GJ Steel H-Sections by Sectioning Method and Method Improvement. Advanced Steel Construction. 2017;13(1), 78-95.

[8] Yong-Lei Xu, Yong-Jiu Shi, Yi-Ran Wu, Ling-Ye Meng. Residual Stress of Welded I Sections Fabricated from High Performance Steel: Experimental Investigation and Modelling. Advanced Steel Construction, 15(1), 1-8, 2019.

[9] Mirzaee-Sisan and A. Welding residual stresses in a strip of a pipe. International Journal of Pressure Vessels and Piping. 2018;159, 28-34.

[10] GUO Zhengxing, ZHU Zhangfeng, NIU Meng. Case Analysis and Warning of Installation Collapse Accidents of Steel Structure. Construction Technology. 2010;39 (07): 35-39.

[11] Ding Y., Qi L., Li Z.X. Mechanical calculation model for welded hollow spherical joint in spatial latticed structures. Advanced Steel Construction. 2011;7(4), 330-343.

[12] Zang Qian, LIU Hongbo, LI Yanbo, CHEN Zhihua, LI Xinghao. Mechanical properties of welded hollow spherical joints reinforced with external ribs under axial tension. Spatial Structures. 2022;28 (01): 71-78.

[13] YU Kequan, YU Jiangtao, TANG Bo. Experimental And Finite Element Analysis on The Ultimate Bearing Capacity of Hollow Spherical Joints with Ribbed Stiffener. Industrial Construction. 2011;41 (08): 85-90.

[14] CHEN Zhihua, WEN Suolin, LIU Hongbo, WANG Xiaodun, HU Hongzhi, HAN Ruijing. A Study on the Mechanical Properties of Large-Size Welded Hollow Spherical Joints of Beijing Daxing International Airport. Progress in Steel Building Structures. 2022;24 (01): 15-23.

[15] Li X. Load-carrying Capacity and Practical Design Method of Welded Hollow Spherical Joints in Space Latticed Structures. Advanced Steel Construction. 2010;6(4), 976-1000.

[16] Liao, J., Zhang, Y., Wu, J. Short-member model of reticulated shell with semi-rigid welded hollow spherical joints for elastic-plastic analysis. World Earthquake Engineering. 2010; 26 (3), 37-42.

[17] LIU Haifeng, LUO Yaozhi, XU Xian. Rigiditty of Welded Hollow Spherical Joints on Finite Element Analysis Precesion of Reticulated Shells. Engineering Mechanics. 2013;30 (01): 350-358+364.

[18] Lopez A, Puente l, Aizpurua H. Experimental and analytical studies on the rotational stiffness of joints for single-layer structures. Engineering Structures. 2010;33 (3): 731-737.

[19] Wang, X., Wang, F. Stiffness analysis of welded spherical joints with rib stiffeners. Applied Mechanics and Materials. 2011;71-78, 3756-3759.

[20] YAN Xiangyu, ZHANG Qiwu, QI Guocai, CHEN Zhihua. Study on bending stiffness of welded hollow spherical joints based on bending loading states. Journal of Experimental Mechanics. 2019; 34 (06): 945-953 .

[21] Yan X, Zhang Y, Chen Z, Liu H, Zhang Q. Flexural capacity and bending stiffness of welded hollow spherical joints with H-beams. Advances in Structural Engineering. 2021;24(5):1024-1039.

[22] Liu Hongbo, Gao Haotian, Chen Zhihua. Research on reinforcing method for welded hollow spherical joints. Journal of Constructional Steel Research. 182, 2021.

[23] Hong-bo Liu, Ying-jie Zhang, Lan Wang, Zhi-hua Chen. Mechanical Performance of Welded Hollow Spherical Joints at Elevated Temperatures. Advanced Steel Construction. 2020;16(1), 1-12.

[24] Lu J, Chen Z, Liu H, Guo Z. Behavior of eccentrically loaded welded hollow spherical joints after elevated-temperature exposure. Advances in Structural Engineering. 2019;22 (6):1352-1367.

[25] ZHAO Zhongwei, WU Gang. Random Compression Capacity of Corroded Whsjs. Engineering Mechanics. 2021;38 (05): 219-228+238.]

[26] Zhao Zhongwei, Dai Bozhi, Xu Hao, Li Tianhe. Bending capacity of corroded welded hollow spherical joints with considering interaction of tension force and bending moment. Structures. 34, 2021.2656-2664

[27] Zhongwei Zhao, Pingyi Zhang, Song Zhou, Xiongtao Fan. Collapse pressure of randomly corroded spherical shell. Ocean Engineering. 2022;246, 110604.

[28] Zhao Zhong Wei, H. Zhu, Z. H. Chen. Mechanical behavior of single-layer reticulated shell connected by welded hollow spherical joints with considering welding residual stress. Welding in the World. 2016;60(1), 61-69.

[29] LIU Mingjiong. Manual of practical mechanical Engineering materials. 2004; China: Liaoning.

[30] LIU Xiaoyu. Magnetic Measurement Method to Test Steel Bridge Welding Residual Stress. Journal of Chongqing Jiaotong University (Natural Science). 2010;29 (01): 38-41+84.